Rare Metal Materials and Engineering
Volume 52, Issue 7, July 2023
Available online at www.rmme.ac.cn

Science Press

Cite this article as: Chen Shanshan, Liu Zongde, Pan Chaoyang, et al. Effect of Si on High-Temperature Corrosion Resistance of Ni-Cr-Mo Alloy Cladding Layer[J]. Rare Metal Materials and Engineering, 2023, 52(07): 2343-2352.

ARTICLE

Effect of Si on High-Temperature Corrosion Resistance of Ni-Cr-Mo Alloy Cladding Layer

Chen Shanshan, Liu Zongde, Pan Chaoyang, Cheng Kehan, Shen Yue

Key Laboratory of Power Station Energy Transfer Conversion and System, Ministry of Education, North China Electric Power University, Beijing 102206, China

Abstract: To investigate the effect of Si content on the high-temperature corrosion resistance of Ni-Cr-Mo alloy cladding layers, four cladding layers with different Si contents were prepared by laser melting technique. The corrosion resistance of the four cladding layers was tested by the mass loss method in a simulated waste-to-energy corrosive environment at different temperatures. Through the analysis about the characteristics of corrosion products of four cladding layers generated at 600 and 650 °C, it is found that the Si addition is beneficial to the stability of the Cr-rich oxide in the corrosion products. The adhesion of Cr-rich oxide to the substrate can also be enhanced through the pinning effect, thus effectively improving the corrosion resistance of cladding layer. However, excess Si addition has the negative effect. When the temperature is above 600 °C, the cladding layer with 3wt% Si shows the optimal corrosion resistance. This phenomenon is attributed to the formation of SiO_2 protective layer in the corrosion layer, which improves the corrosion resistance of cladding layer with 3wt% Si. Because of the small Si addition amount and the severe Si segregation, the effective SiO_2 protective layer cannot be formed in the cladding layers with 1wt% and 5wt% Si, respectively.

Key words: high-temperature corrosion; Si content; Ni-Cr-Mo; laser cladding

Waste incineration is widely used nowadays as one of the main methods of domestic waste disposal. The transformation mechanism from waste incineration into electricity is mainly through the resource integration of municipal domestic waste: the waste is fully burned in a high-temperature and high-pressure environment, and the heat released during the incineration process drives the formation of high-temperature water vapor, thereby generating electricity by turbine. This approach achieves the goal of waste cleaning and realizes the recycling of domestic resources[1–3]. However, due to the complex composition of domestic waste, sulfate and hydrochloride are produced during the high-temperature combustion process. The acidic gases (SO_2, SO_3, and HCl) may be released when the melted salts react with the metals in the furnace, therefore producing sulfides or chlorides. During boiler operation, the outer ash slag can be removed by ash cleaning. However, if the ash slag is too thick, the resultant alkali metal sulfides and chlorides are exposed to high-temperature flame in the subsequent decomposition reactions. Thus, a new critical reaction surface is generated. In the environment of acidic gas, the tube wall is continuously corroded, which eventually leads to the blast of tube wall[4–7]. High-temperature corrosion increases the accident possibility and restricts the development of waste incineration technique. Therefore, it is crucial to solve the high-temperature corrosion in waste incineration boilers.

The protection for power plants against high-temperature corrosion has attracted extensive attention[8–10]. The protective layer of precious metal material is usually prepared on the substrate surface through laser cladding technique by high-energy and high-density laser beam. This method has the advantages of no crack/hole, good metallurgical bonding with substrate, and low dilution rate, which can significantly improve the wear resistance, corrosion resistance, heat resistance, and oxidation resistance of the substrate surface[11–14]. The selection and development of material are important to enhance the corrosion resistance of cladding layers and prolong the service life of boiler tube. Ni-Cr-Mo

Received date: December 26, 2022
Foundation item: General Fund Project in Equipment Pre-research Field (61409220202)
Corresponding author: Liu Zongde, Ph. D., Professor, Key Laboratory of Power Station Energy Transfer Conversion and System, Ministry of Education, North China Electric Power University, Beijing 102206, P. R. China, Tel: 0086-10-61772812, E-mail: lzd@ncepu.edu.cn

alloys have excellent corrosion resistance in the corrosive oxidization and reduction environments due to the addition of Cr and Mo into the Ni-based alloys[15–16]. The addition of trace elements can further reduce the degradation rate of materials under high-temperature corrosion by improving the adhesion and changing the growth mechanism of oxides. Si shows great potential as an additive[8,17–19]. Si can form silicides with Ni and Cr elements in the alloy; it promotes the coexistence of metallic and covalent bonds, forms strong atomic bonding, and enhances the chemical stability, thereby improving the corrosion resistance of alloys.

Chen et al[20] investigated the microstructure, phase composition, and high-temperature corrosion resistance of Ni-Cr-Mo alloy cladding layers with different Si contents in the mixture environment containing chloride and sulfate salts at 550 °C. However, with increasing the boiler operation parameters, the corrosion caused by high temperature inevitably becomes more serious. Therefore, it is necessary to analyze the corrosion resistance of cladding layers at higher temperatures. In this research, the effect of Si content on the high-temperature corrosion resistance of Ni-Cr-Mo alloy cladding layers at different corrosion temperatures was investigated, and the optimal addition amount of Si in the cladding layer was discussed. This research provides guidance for the protection for waste incineration power plants against the high-temperature corrosion and optimizes the design of Ni-Cr-Mo alloy cladding layer.

1 Experiment

Ni-Cr-Mo-Si cladding layers with different Si contents were deposited on Q235 steel by laser cladding technique, and the specimens with 0wt% , 1wt% , 3wt% , and 5wt% Si were named as S0, S1, S3, and S5, respectively. The chemical composition of specimens is shown in Table 1. The powder preparation process and the operation parameters of laser cladding were according to the methods in Ref. [20]. The cladding layer with thickness of over 4 mm was obtained by dense overlapping of multiple channels. To avoid the dilution effect of substrate elements on the cladding layer, wire cutting was conducted in the upper-middle region of the cladding layer to obtain the specimens with size of 20 mm×10 mm×2 mm. Before the experiment, the specimens were ground by sandpaper and cleaned by ethanol solution and acetone solution.

To simulate the complex corrosion environment caused by waste combustion, NaCl, KCl, Na_2SO_4, and K_2SO_4 were mixed at the mass fraction ratio of 1: 1: 1: 1 as molten salt corrosion reagents, and the high-temperature corrosion tests were conducted at 500, 600, and 650 °C. To explore the influence of Si element on the corrosion resistance of cladding layer, the mass loss rate per unit area (m) of corroded specimens was measured to characterize the corrosion resistance of different specimens. The calculation formula is as follows:

$$m = \frac{m_0 - m_1}{S} \quad (1)$$

where m_0 is the initial mass of the experimental specimens (g); m_1 is the remaining mass of the specimens after the corrosion test is completed and the corrosion products on the specimen surface are removed; S is the contact area between the specimen surface and corrosive environment (m^2).

During the high-temperature corrosion tests, the as-prepared specimens were placed in dry alumina crucible with mixed salt, and the specimen surface was covered completely by the mixed salt until the crucible was filled. The crucible was placed in the center of the constant-temperature tubular furnace to ensure the uniform corrosion temperature. The corrosion test was conducted for 24, 48, 72, 96, 120, 144, and 168 h. The specimens were taken out from the furnace for acid pickling and mass measurement. The corrosion morphologies were analyzed by X-ray diffractometer (XRD, Raku D/MAX-2400) and scanning electron microscope (SEM, Quanta 200F). The acid pickling process was as follows: the specimens were cooled to room temperature, ultrasonically cleaned by deionized water to remove the corrosive agent and corrosion products on the surface, and ultrasonically cleaned by 25wt% hydrochloric acid (8.082 mol/L) in water bath at 80 °C for 30 min to remove the corrosion products on the specimen surface. After acid pickling process, the specimen mass was measured by electronic balance (accuracy of ±0.01 mg).

XRD was used to analyze the phase components of the corrosion products. SEM coupled with X-ray energy dispersive spectrometer (EDS, Bruker) was used to observe the surface corrosion morphology and element composition of the cladding layers after corrosion. The section morphologies and element distributions after corrosion were also analyzed.

Table 1 Chemical composition of Ni-Cr-Mo-Si cladding layers (wt%)

Specimen	Cr	Mo	Si	Ni
S0	24.0	13.0	0.0	Bal.
S1	24.0	13.0	1.0	Bal.
S3	24.0	13.0	3.0	Bal.
S5	24.0	13.0	5.0	Bal.

2 Results and Discussion

2.1 High-temperature corrosion kinetics

Fig. 1 shows the mass loss curves of four cladding layers with different Si contents corroded in mixed salt at 500, 600, and 650 °C for 168 h. At 500 and 600 °C, the mass loss curves of four cladding layers show the parabolic patterns, whereas those at 650 °C show the linear pattern. The fitting equations of the mass loss of cladding layers during corrosion at different temperatures are shown in Table 2. The corrosion rate at 650 °C is significantly higher than that at 500 and 600 °C.

At 500 °C, the corrosion rate of cladding layers can be arranged as S0>S1>S3>S5; whereas at 600 and 650 °C, the corrosion rate of cladding layers is arranged as S0>S1>S5>

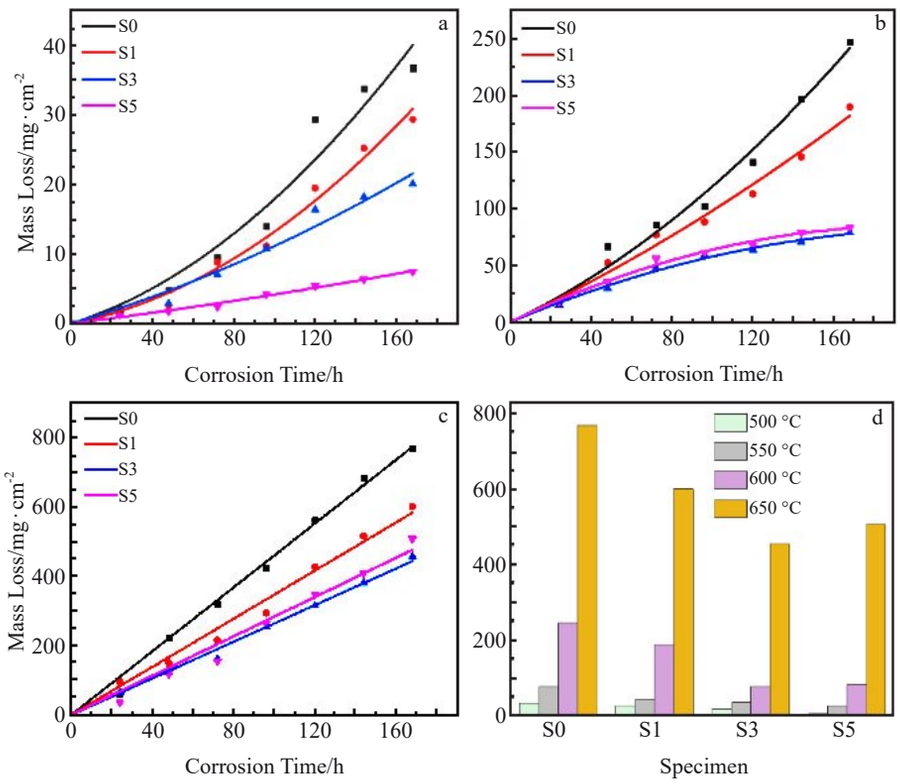

Fig.1 Mass loss curves of cladding layers with different Si contents at 500 °C (a), 550 °C (b), and 600 °C (c); mass loss comparison of cladding layers with different Si contents after corrosion at different temperatures for 168 h (d)

Table 2 Fitting equations of mass loss curves of different cladding layers during corrosion at different temperatures

Temperature/°C	Specimen	Fitting equation
500	S0	y=0.091 45x+0.000 877 5x^2
	S1	y=0.055 78x+0.000 764 0x^2
	S3	y=0.086 24x+0.000 252 1x^2
	S5	y=0.036 8x+0.000 499 9x^2
600	S0	y=0.843 1x+0.003 56x^2
	S1	y=0.835 4x+0.001 49x^2
	S3	y=0.746 3x−0.001 69x^2
	S5	y=0.852 5x−0.002 15x^2
650	S0	y=4.611 96x
	S1	y=3.479 65x
	S3	y=2.647 08x
	S5	y=2.841 89x

S3. In addition, it is worth noting that at 600 °C, the quadratic coefficients of the fitting curves of S3 and S5 specimens are negative, indicating that the corrosion rates of S3 and S5 specimens are effectively suppressed in the later stage of corrosion at 600 °C. Fig. 1d shows the mass loss comparison of cladding layers with different Si contents after corrosion at different temperatures for 168 h. It can be seen that the final mass loss of S0, S1, S3, and S5 specimens is 36.78, 29.40, 20.12, and 7.46 mg/cm^2 at 500 °C, respectively. The corrosion rate of the cladding layers is decreased significantly with increasing the Si content, and the cladding layer with 5wt% Si exhibits the optimal corrosion resistance at 500 °C. The mass loss of S5 specimen is only 20.3% of that of S0 specimen.

At 600 °C, the final mass loss of S0, S1, S3, and S5 specimens is 247.48, 189.99, 78.81, and 83.37 mg/cm^2, respectively. It can be seen that S3 specimen exhibits the optimal corrosion resistance at 600 °C, and the final mass loss of S3 specimen is only 31.8% of that of S0 specimen.

When the temperature increases to 650 °C, the mass loss of all cladding layers increases significantly and the mass loss curves are approximately linear. Briefly, the mass loss is continuously increased with increasing the corrosion time. The final mass loss of S0, S1, S3, and S5 specimens is 770.90, 602.77, 457.51, and 508.42 mg/cm^2, respectively. As a result, the corrosion rate of different cladding layers varies drastically with further incresaing the corrosion temperature.

When the corrosion temperature increases from 500 °C to 650 °C, the corrosion rate of S0, S1, S3, and S5 specimens increases by 20.96, 20.50, 22.73, and 68.18 times, respectively. Particularly, at 650 °C, the corrosion resistance of S3 specimen is obviously better than that of other cladding layers. This result is similar to that in Ref. [21]: during high-temperature oxidation at 1000 °C, the Ni-Cr-Al alloy with 6wt% Si shows better oxidation resistance than that with 2wt% Si does, but presents worse oxidation resistance than that with 4wt% Si does. According to the mass loss of

cladding layers at different temperatures, the mass loss of the Ni-Cr-Mo alloy cladding layers with Si addition is generally much smaller than that without Si addition, suggesting that Si addition is beneficial to improve the corrosion resistance of the cladding layers at high temperatures. However, excess Si addition may result in negative effect.

Because the investigation of corrosion resistance of cladding layers at even higher temperatures is more meaningful, the subsequent discussions will only focus on the characteristics of corrosion products at 600 and 650 °C.

2.2 Products after high-temperature corrosion

Fig. 2 shows XRD patterns of corrosion products of different cladding layers after corrosion at 600 and 650 °C for 168 h. It can be seen that at 600 and 650 °C, in addition to Ni and Cr oxides, such as NiO and Cr_2O_3, the composite oxides, such as $NiCr_2O_4$ and $NiMoO_4$, are formed on the surfaces of cladding layers, which indicates that the solid-state reactions between the oxides occur among NiO, Cr_2O_3, and MoO_2. Some Ni atoms replace Cr and Mo in the oxide skins, which results in the mass loss of specimens. Additionally, SiO_2 can be detected in the corrosion products of cladding layers with Si addition, which is beneficial to the enhancement in corrosion resistance. At 650 °C, $NiCrO_4$ can also be detected in the corrosion products of cladding layer surfaces. This is because at 650 °C, the mixed salts all melt, providing a good medium for ion transfer, and the SO_4^{2-} ions in the molten salt decompose to form O^{2-}, thereby promoting the formation of CrO^{4-}.

2.3 Surface morphology after high-temperature corrosion

Fig.3 and Fig.4 show the morphologies of surface corrosion products of cladding layers with different Si contents after continuous corrosion at 600 and 650 °C for 168 h, respectively. It can be seen that at 600 °C, a large number of granular corrosion products appear on the corrosion surface with the laminar distribution. Combined with EDS analysis results in Table 3, it is found that two corrosion product layers are formed on the specimen surface. The content of Cr and O elements of one corrosion product layer is much higher than that of other elements. It can be inferred that a dense Cr_2O_3 film is formed on the cladding layer surface, which prevents the further diffusion of O, S, Cl, and other corrosive agents into the substrate and retards the corrosion. The other corrosion product layer mainly consists of Ni and O, which is caused by selective corrosion and dissolution of Cr-rich oxides. With increasing the Si content, the corrosion product layer on the specimen surface becomes more uniform and denser. Obvious cracks can be observed on the product layers of S0 and S1 specimen surfaces. However, no cracks can be observed on S3 and S5 specimens, indicating that the sufficient addition of Si element promotes the formation of dense Cr_2O_3 layer on the surface of cladding layer, which improves the corrosion resistance of cladding layer[21].

It is worth noting that when the Si content is 3wt%, the Si content in the Cr-rich and Ni-rich oxides on the surface of cladding layers increases significantly. However, when the Si content further increases to 5wt% , the Si content only increases in the Cr-rich oxides, according to the comparison of element contents among positions 6 – 9 in Table 3. It is demonstrated that because laser cladding involves the rapid heating and cooling processes, the high solidification rate prevents the adequate diffusion of Cr, Mo, Si, and other elements, leading to the interdendritic segregation. Particularly, the element distribution in S5 specimen is very heterogeneous: Si is significantly enriched in the beige phase between the dendritic crystals[20]. This result may explain the phenomenon that the protective SiO_2 film cannot be formed on S5 specimen, therefore leading to worse corrosion resistance of S5 specimen, compared with that of S3 specimen.

At 650 °C, the corrosion is intensified, and the corrosion rate of cladding layers increases significantly. The surface corrosion products are sparse and porous, producing corrosion cracks. The S0 specimen suffers the most severe corrosion, and it already presents obvious grooves, as shown in Fig. 4a. The corroded surface of S0 specimen shows longitudinal pattern of lap traces during the formation of cladding layer. The presence of cracks not only accelerates the cracking and spalling of corrosion products, but also provides good

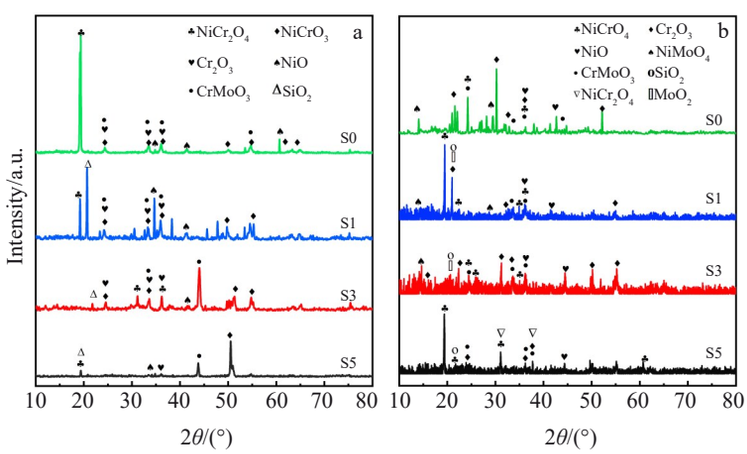

Fig.2 XRD patterns of corrosion products after corrosion at 600 °C (a) and 650 °C (b) for 168 h

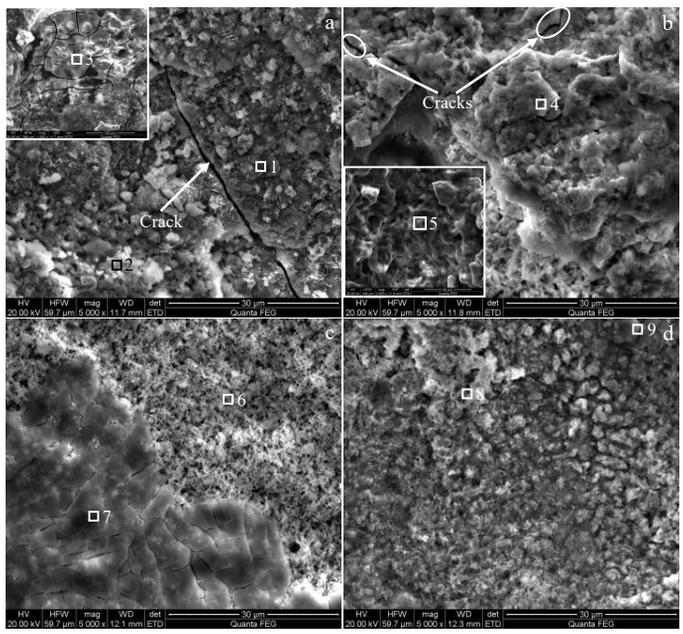

Fig.3 Surface morphologies of corrosion products on S0 (a), S1 (b), S3 (c), and S5 (d) cladding layer specimens after corrosion at 600 °C for 168 h

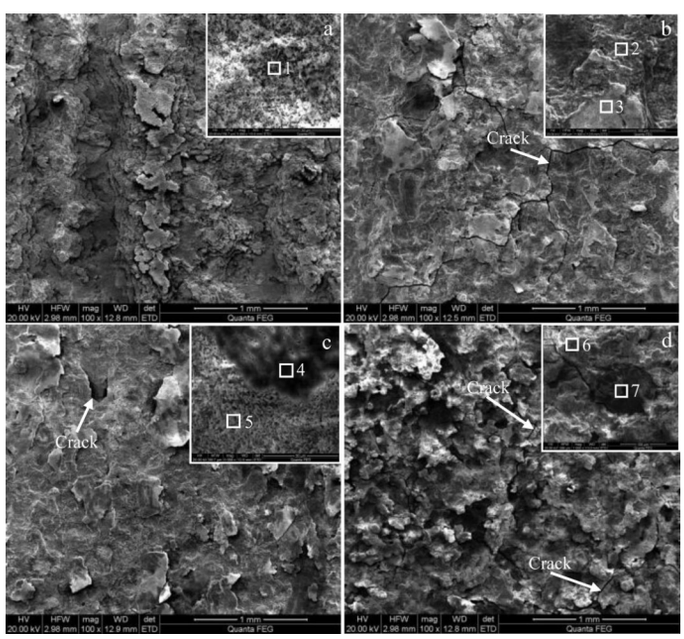

Fig.4 Surface morphologies of corrosion products on S0 (a), S1 (b), S3 (c), and S5 (d) cladding layer specimens after corrosion at 650 °C for 168 h

diffusion channels for elements, such as O, Cl, and S. The corrosive agent can further corrode the interior material through the cracks and produce new corrosion products. According to EDS analysis results in Table 4, O, Cr, and Ni with high contents can be found in the corrosion products. Combined with XRD analysis results, it is inferred that the solid-state reaction occurs between NiO and Cr_2O_3 in the product layer, thereby generating $NiCr_2O_4$. In addition, the Ni and O contents in the black granular phase at position 7 are very high, indicating the existence and location of granular NiO phase. This result indicates that the selective corrosion occurs at position 7, which is also consistent with XRD analysis results. With the corrosion reaction proceeding, the Cr-rich oxides in the surface corrosion products are preferentially dissolved, consuming a large amount of oxygen and reducing the nearby oxygen partial pressure. This phenomenon destroys the dense structure of the oxide film and provides a good channel for the diffusion of O, S, and Cl

Table 3 EDS analysis results of different positions in Fig.3 (wt%)

Position	Ni	Cr	Mo	Si	O	Cl	S
1	07.15	58.83	04.54	-	27.67	01.09	00.71
2	05.50	50.88	06.34	-	36.20	01.07	00.00
3	60.91	01.43	00.73	-	26.96	08.97	00.99
4	07.24	55.17	04.19	01.62	31.07	00.71	00.00
5	40.37	09.64	12.78	00.24	33.32	00.30	03.35
6	24.47	31.96	01.78	04.00	36.62	01.16	00.00
7	33.34	22.40	03.48	05.01	34.63	00.90	00.23
8	15.29	39.87	03.11	02.02	37.75	01.20	00.76
9	24.45	25.80	08.34	00.98	38.28	01.12	01.02

Table 4 EDS analysis results of different positions in Fig.4 (wt%)

Position	Ni	Cr	Mo	Si	O	Cl	S
1	04.00	49.69	01.62	-	43.29	01.09	00.31
2	17.97	25.41	08.23	00.44	45.32	00.94	01.69
3	06.75	49.83	01.94	00.87	38.45	01.64	00.51
4	23.62	25.87	09.37	00.34	38.01	00.75	02.04
5	10.83	51.00	02.28	00.73	32.73	01.56	00.88
6	17.88	29.26	05.15	02.51	42.90	00.95	01.35
7	56.08	01.40	02.74	00.27	30.51	08.70	00.29

to the inner alloy, thus accelerating the corrosion and increasing the corrosion mass loss.

2.4 Cross-sectional morphology after high-temperature corrosion

To further investigate the corrosion characteristics of the Ni-Cr-Mo cladding layers with different Si contents, the cross-sectional morphologies of different cladding layers after corrosion at 600 °C for 168 h are observed, as shown in Fig.5. The element distributions in corrosion products of different cladding layers are also shown in Fig. 5, which further confirms that the surface corrosion products are mainly composed of Cr_2O_3. Additionally, Cr is continuously diffused outwards from the substrate to the outer side, and it is gradually consumed, which is not conducive to the formation of a long-term protective Cr_2O_3 oxide skin. With the corrosion proceeding, Cr continuously diffuses from the substrate to the surface, forming a Cr-dissipative zone. The thickness of the outermost corrosion product on the S0 specimen surface reaches about 320 μm. In addition, the penetration cracks can be found in the corrosion product layers of S0 and S1 specimens, which provide a good channel for the corrosive medium into the substrate, thereby decreasing the protective effect of the Cr-rich oxide skin and leading to severe corrosion. The outer sides of S3 and S5 cladding layers produce thin and dense Cr-rich oxides with pinning effect, which promotes better adhesion between the oxides and substrate and improves the protection effect. These phenomena all suggest that Si addition contributes to the stability of Cr-rich oxides and decreases the corrosion mass loss of cladding layers. In addition, Si and O are concentrated near the substrate of S3 specimen (the innermost part of the corrosion product). Combined with XRD result, it can be inferred that the continuous SiO_2 film is generated at this area, which further hinders the corrosion reaction. As a result, S3 specimen exhibits the optimal corrosion resistance.

2.5 Corrosion mechanism of cladding layer

The high-temperature corrosion of heating tube in waste incineration power plant is a complex process, and the corrosion caused by molten salt usually includes the chemical corrosion, electrochemical corrosion, interface corrosion, and oxide dissolution. It is well known that the corrosion resistance of metals and alloys at high temperatures usually depends on the reaction of protective oxide scales. In this research, the high-temperature corrosion environment of molten salt in waste incineration power plant was simulated.

At lower temperatures (500–550 °C), the corrosion medium partially melts, and the chemical corrosion is still the main corrosion mechanism. The corrosion occurs in the air atmosphere, and O_2 can freely react with the cladding layer through the unmelted corrosive medium. The related chemical reactions at the initial corrosion stage are as follows:

$$xM\,(s)+y/2O_2\,(g)\rightarrow M_xO_y\,(s) \quad (2)$$

where M is the metal elements (Ni, Cr, Mo, Si). NiO, Cr_2O_3, MoO_2, SiO_2, and other oxides are generated and attached to the surface of cladding layers to provide the protection functions. The oxidation order of different alloying elements depends on the Gibbs free energy (ΔG) at different temperatures. A negative Gibbs free energy indicates that the reaction tends to proceed spontaneously, and a positive small Gibbs free energy indicates the high probability of the reaction occurrence. The reactions with 1 mol O_2 and the related Gibbs free energies at different temperatures to form corresponding metal oxides are shown in Fig.6. It can be seen that the generation of SiO_2 has the lowest Gibbs free energy, and that of Cr_2O_3 has relatively low Gibbs free energy. The generation of MoO_3 is more difficult than that of MoO_2, and NiO is the most difficult to synthesize. Based on these results, SiO_2 should be generated firstly during the oxidization process of cladding layers in this research. Besides, SiO_2, Cr_2O_3, MoO_2, and NiO can all be detected. Since the content of Ni and Cr is much higher than that of Si, Cr is still preferentially oxidized into Cr_2O_3. Oxide layers dominated by Cr_2O_3 can be found in all specimens. In addition, the denseness of the oxide films formed by Cr_2O_3 is better than that formed by Ni oxide[22]. According to Fig. 5, only S3 specimen produces continuous SiO_2 protective layer at 600 °C. This is because the Si content in S1 specimen is too low. Therefore, the oxidation of Ni and Cr still occurs before Si. However, it is worth noting that the S5 specimen with high Si content still fails to produce the continuous Si-rich protective oxide layer. Therefore, it can be concluded that S3 specimen has the optimal Si content, because Si exists more evenly in the dendrite and interdendrite phases, which is beneficial to the formation of continuous SiO_2 protective layer. For S3 specimen, the difference in Si content between the dendrite and interdendrite phases is about 1.43wt%, whereas that in S5 specimen is about 3.47wt%,

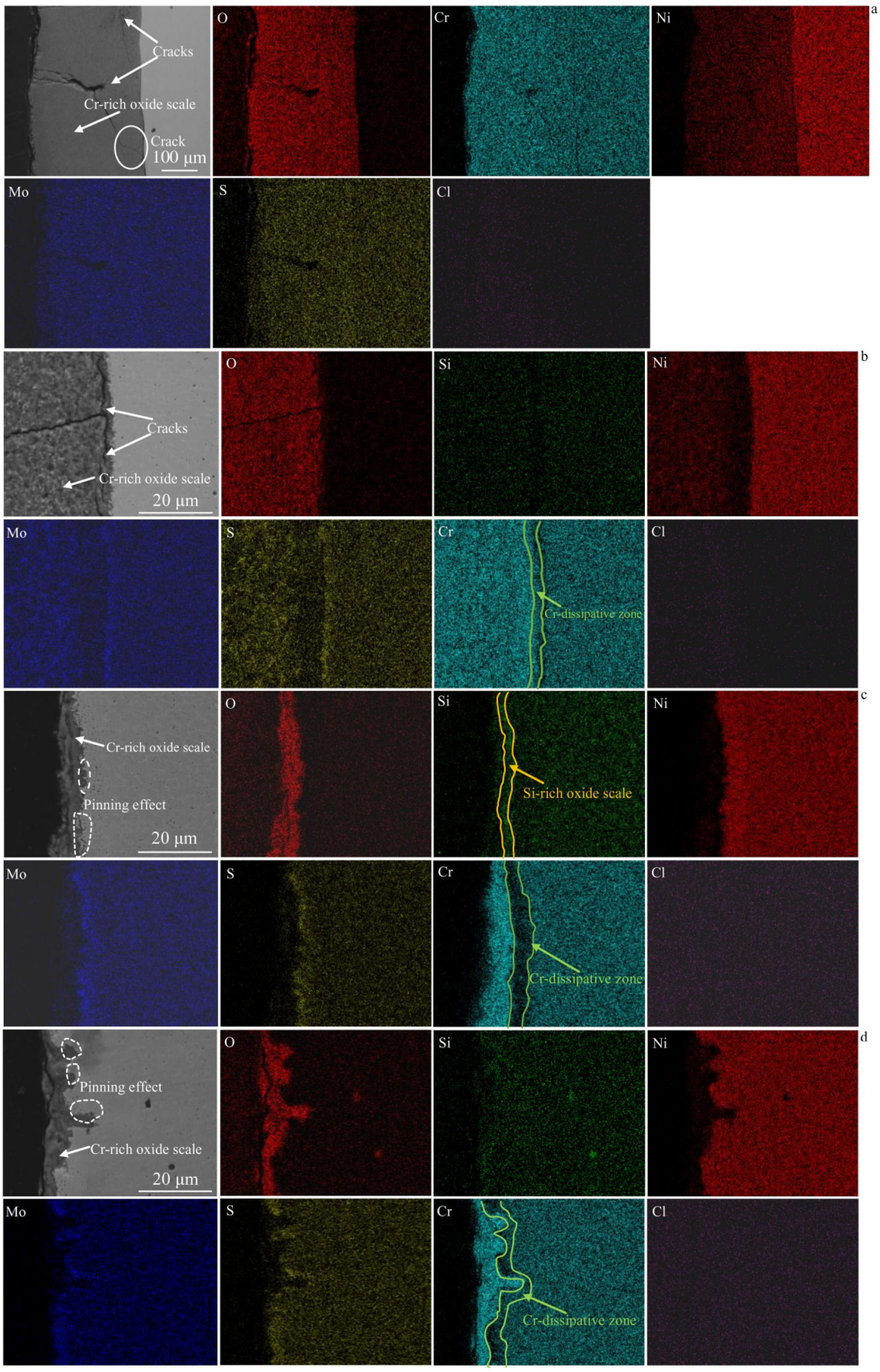

Fig.5 Cross-sectional morphologies and corresponding EDS element distributions of corrosion products on S0 (a), S1 (b), S3 (c), and S5 (d) cladding layer specimens after corrosion at 600 °C for 168 h

which increases by about 2.43 times. The significant non-uniform distribution of Si in S5 specimen may cause the failure in formation of continuous Si-rich oxide layer, thereby decreasing the corrosion resistacne.

At high corrosion temperatures (600 and 650 ° C), the corrosion of different cladding layers is significantly intensified, and the mixed salts are all melted. The liquid molten salt can be considered as an electrolyte, being a good medium for ion transference. In this case, the electrochemical corrosion plays a major role[23]. The SO_4^{2-} ions in the molten salt decompose, as follows:

$$SO_4^{2-} \rightarrow O^{2-} + SO_2 + 1/2O_2 \quad (3)$$

Afterwards, O^{2-} increases in the molten salt environment and the alkaline dissolution reaction occurs on the oxide scale of the cladding layer, as follows:

$$Cr_2O_3 + 3/2O_2 + 2O^{2-} \rightarrow 2CrO_4^{2-} \quad (4)$$

$$2MoO_2 + O_2 + 2O^{2-} \rightarrow 2MoO_4^{2-} \quad (5)$$

$$SiO_2 + 2O^{2-} \rightarrow SiO_3^{2-} \quad (6)$$

The Gibbs free energy curves for the alkaline dissolution of different oxides are also illustrated in Fig. 6. Based on the consumption of 1 mol oxide, the alkaline dissolution of SiO_2 has the highest Gibbs free energy. Thus, the SiO_2-dominated oxide film can provide more powerful protection. Alkaline dissolution of Cr_2O_3 also requires high Gibbs free energy, indicating that it is unstable. According to the cross-section morphologies of S0 and S1 specimens after corrosion at 600 ° C, it can be seen that although the effective Si-rich oxide layer cannot be formed, the thick Cr-rich oxide layer with cracks can be observed on the cladding layer surface. Therefore, Cr_2O_3 and MoO_2 are preferentially consumed. The generation of CrO_4^{2-} and MoO_4^{2-} through the abovementioned reactions can reduce the activity of O^{2-} in the molten salt, so the dissolution of NiO is restrained. Therefore, the Ni-rich oxide can be detected, as shown in Fig.4. With the alkaline dissolution reaction proceeding, the denseness of the surface oxide is reduced, resulting in the unstable protective oxide and thus decreasing the corrosion resistance of cladding layers.

It is reported that the addition of alkali metal chloride salts into the sulfate may substantially increase the corrosion intensity of the alloy. In this research, NaCl and KCl can destroy the protective oxide scales, such as Cr_2O_3 on the cladding layer surface. Thus, the related reactions[24–25] are as follows:

$$Cr_2O_3 + 4RCl + 2.5O_2\ (g) = 2R_2CrO_4 + 2Cl_2\ (g) \quad (7)$$

$$RCl\ (s, g) + H_2O\ (g) \rightarrow ROH\ (s, g) + HCl\ (g) \quad (8)$$

$$4HCl\ (g) + O_2\ (g) \rightarrow 2Cl_2\ (g) + 2H_2O\ (g) \quad (9)$$

where R refers to the alkali metal elements (Na, K). These reactions occur during the corrosion process, and therefore Cl_2 and HCl are produced.

It is demonstrated that Cl_2 can react with the cladding layer through the oxide on the surface to produce chlorides[10,26]. Fig. 6b shows the Gibbs free energies for the reaction of different metallic elements with Cl_2 to form the metal

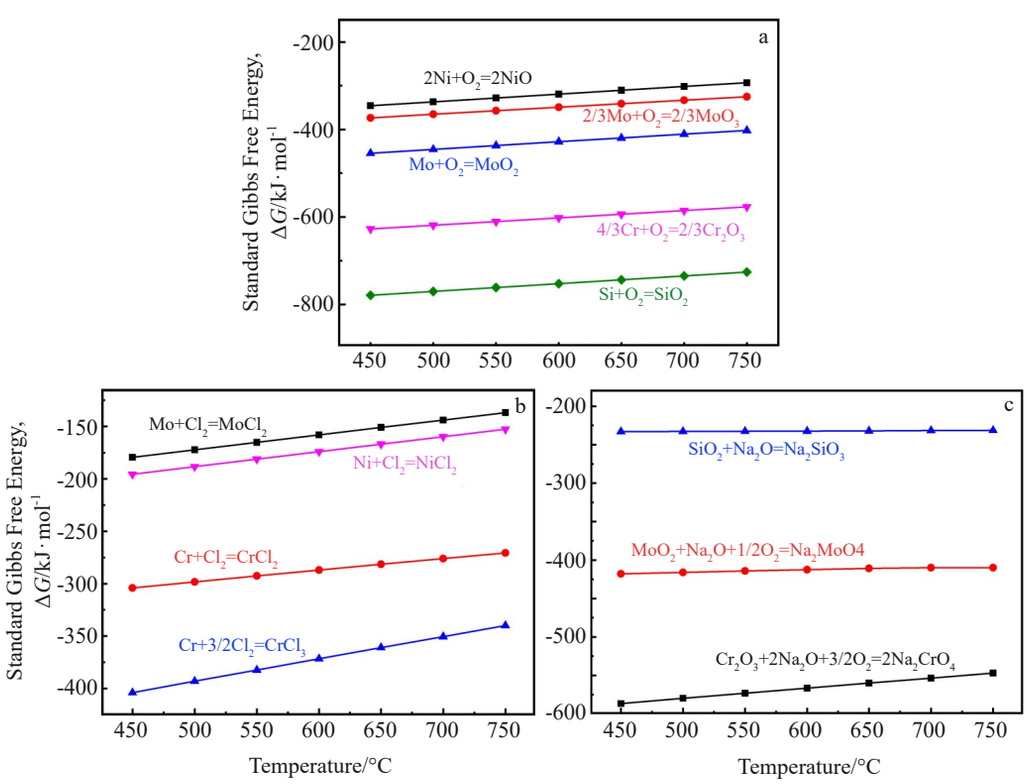

Fig.6 Standard Gibbs free energies of different reactions at different temperatures: (a) oxidization reactions; (b) chloride reactions; (c) mixture reactions

chlorides, and the ΔG value can arranged as Cr<Ni<Mo. So, the Mo element can enhance the corrosion resistance of the cladding layer against Cl_2. The vapor pressure of these chlorides is high even at low temperatures. The higher the temperature, the more volatile the products and the more intense the corrosion. In this research, the larger the distance away from the alloy surface, the higher the O_2 activity. Additionally, when the chlorides diffuse to the area with stable O_2 partial pressure, they will be transformed into the corresponding oxides[27], as follows:

$$M\,(s)+Cl_2\,(g)\rightarrow MCl_2\,(s) \quad (10)$$

$$M\,(s)+2HCl\,(g)\rightarrow MCl\,(s)+H_2\,(g) \quad (11)$$

$$MCl\,(s)\rightarrow MCl\,(g) \quad (12)$$

$$xMCl_2\,(g)+y/2O_2(g)\rightarrow M_xO_y\,(s)+xCl_2\,(g) \quad (13)$$

Partial Cl_2 generated by the reaction will diffuse back to the cladding layer surface. Therefore, the reaction proceeds for a long time. This is because the newly generated oxide is porous without protection, which may easily react with Cl_2. Besides, the newly generated oxide may grow as the weak position of the overall oxide scale, which increases the internal stress of the oxide and destroys the protection of the oxide. Additionally, these phenomena may cause a large number of cavities in the interface between oxide scale and cladding layer. The rapid peeling of the oxide scale may also occur, resulting in serious corrosion.

3 Conclusions

1) In the simulated waste-to-energy environment at high-temperatures, the Ni-Cr-Mo alloy cladding layer with Si addition produces a dense chromium-rich oxide skin on the surface to prevent the further corrosion. With the corrosion proceeding, Cr continuously diffuses from the substrate to the surface, forming a Cr-dissipative zone.

2) The Si addition can effectively improve the high-temperature corrosion resistance of Ni-Cr-Mo alloy, and the corrosion resistance of Ni-Cr-Mo alloy cladding layer with 3wt% Si above 600 °C is optimal. Ni-Cr-Mo alloy cladding layer with 5wt% Si has excellent corrosion resistance when the corrosion temperature is below 550 °C, and that with 3wt% Si shows optimal corrosion resistance when the temperature is above 600 °C.

3) The increase in Si content not only contributes to the stability of the Cr-rich oxide scale, but also enhances the bonding between the Cr-rich oxide scale and the substrate through the pinning effect. SiO_2 protective layer is formed beneath the Cr-rich oxide scale of Ni-Cr-Mo alloy cladding layer with 3wt% Si, which contributes to the enhancement in corrosion resistance of cladding layer.

References

1 Wang G Y, Liu H, Chen T Z *et al*. *Corrosion Science*[J], 2021, 189: 109 592

2 Varjani S, Shahbeig H, Popat K *et al*. *Bioresource Technology*[J], 2022, 355: 127 247

3 Sun H F, Liu J. *Engineering Failure Analysis*[J], 2022, 133: 105 964

4 Yang Bo, Zhong Zhiqiang, Huang Qiaoxian *et al*. *Guangdong Electric Power*[J], 2016, 29(6): 5 (in Chinese)

5 Zahrani E M, Alfantazi A M. *Corrosion Science*[J], 2014, 85: 60

6 Chen G Y, Wenga T, Ma W C *et al*. *Applied Energy*[J], 2019, 247: 630

7 Yan Z R, Wang L, Li X C *et al*. *Engineering Failure Analysis*[J], 2022, 140: 106 457

8 Liu C C, Liu Z D, Gao Y *et al*. *Applied Surface Science*[J], 2022, 578: 152 061

9 Chen L, Zhang X Z, Wu Y *et al*. *Corrosion Science*[J], 2022, 201: 110 271

10 Liu S N, Liu Z D, Wang Y T *et al*. *Corrosion Science*[J], 2014, 83: 396

11 Singh S, Goyal D K, Kumar P *et al*. *International Journal of Refractory Metals and Hard Materials*[J], 2022, 105: 105 825

12 Abioye T E, McCartney D, Clare A T. *Journal of Materials Processing Technology*[J], 2015, 217: 232

13 Yuan Wuyan, Li Ruifeng, Chen Zhaohui *et al*. *Surface and Coatings Technology*[J], 2021, 405: 126 582

14 Wang X Y, Liu Z D, Li J Y *et al*. *Optik*[J], 2022, 270: 169 930

15 Guo C, Shi S W, Dai H L *et al*. *Engineering Failure Analysis*[J], 2022, 140: 106 580

16 Zhu H L, Muránsky O, Wei T *et al*. *Materialia*[J], 2021, 16: 101 069

17 Dong Z Q, Li M, Behnamian Y *et al*. *Corrosion Science*[J], 2020, 166: 108 432

18 Liu H X, Huang F, Yuan W *et al*. *Corrosion Science*[J], 2020, 173: 108 758

19 Liu J, Chen Y, Zhang J. *Surface and Coatings Technology*[J], 2019, 375: 903

20 Chen S S, Liu Z D, Shen Y *et al*. *Materials*[J], 2022, 15(9): 3152

21 Wang S, Wu Y, Ni C S *et al*. *Corrosion Science*[J], 2009, 51(3): 511

22 Sundman B, Jansson B, Andersson J O. *Calphad*[J], 1985, 9(2): 153

23 Wang J H, Li D G, Shao T M. *Corrosion Science*[J], 2022, 200: 110 247

24 Kassim S A, Thor J A, Seman A A *et al*. *Corrosion Science*[J], 2020, 173: 108 761

25 Reddy L, Sattari M, Davis C J *et al*. *Corrosion Science*[J], 2019, 153: 108 076

26 Pettersson J, Folkeson N, Johansson L *et al*. *Oxidation of Metals*[J], 2011, 76(1–2): 93

27 Ruh A, Spiegel M. *Corrosion Science*[J], 2006, 48(3): 679

Si对Ni-Cr-Mo合金熔覆层高温耐腐蚀性能的影响

陈珊珊，刘宗德，潘朝阳，程可翰，申　越
(华北电力大学 电站能量传递转化与系统教育部重点实验室，北京 102206)

摘　要：为研究Si含量对Ni-Cr-Mo系合金熔覆层耐高温腐蚀性能的影响，利用激光熔覆技术制备了4种不同Si含量的熔覆层。采用失重法测试了4种熔覆层在模拟垃圾发电腐蚀环境中多种温度下的耐腐蚀性能。通过对4种熔覆层在600及650 ℃下腐蚀产物的特性分析，发现Si的加入有助于腐蚀产物中富Cr氧化皮的稳定性。还可以通过“钉扎”作用提升富Cr氧化皮与基体的粘结性，从而有效提高熔覆层的耐腐蚀性能。但Si含量并非越多越好。当温度提升到600 ℃以上，含3%（质量分数，下同）Si的合金展现了最佳的耐腐蚀性能。这是由于含3% Si的合金腐蚀层中形成了一层保护性的SiO_2，有助于耐腐蚀性能的提升。而含1% Si的合金由于Si含量较低，含5% Si的合金由于Si的偏析严重，均未能形成有效的SiO_2保护层。

关键词：高温腐蚀；Si含量；Ni-Cr-Mo；激光熔覆

作者简介：陈珊珊，女，1987年生，博士，华北电力大学电站能量传递转化与系统教育部重点实验室，北京 102206，电话：010-61772277，E-mail：10602054@ncepu.edu.cn